

Spatio-Temporal Graph Convolution for Functional MRI Analysis

Soham Gadgil^{*,1}, Qingyu Zhao^{*,2}, Ehsan Adeli^{1,2}, Adolf Pfefferbaum^{2,3},
Edith V. Sullivan², Kilian M. Pohl^{2,3}

¹ Computer Science Department, Stanford University, Stanford, USA

² School of Medicine, Stanford University, Stanford, USA

³ Center of Health Sciences, SRI International, Menlo Park, USA

Abstract. The BOLD signal of resting-state fMRI (rs-fMRI) records the functional brain connectivity in a rich dynamic spatio-temporal setting. However, existing methods applied to rs-fMRI often fail to consider both spatial and temporal characteristics of the data. They either neglect the functional dependency between different brain regions in a network or discard the information in the temporal dynamics of brain activity. To overcome those shortcomings, we propose to formulate functional connectivity networks within the context of spatio-temporal graphs. We then train a spatio-temporal graph convolutional network (ST-GCN) on short sub-sequences of the BOLD time series to model the non-stationary nature of functional connectivity. We simultaneously learn the graph edge importance within ST-GCN to enable interpretation of functional connectivities contributing to the prediction model. In analyzing the rs-fMRI of the Human Connectome Project (HCP, $N=1,091$) and the National Consortium on Alcohol and Neurodevelopment in Adolescence (NCANDA, $N=773$), ST-GCN is significantly more accurate than common approaches in predicting gender and age based on BOLD signals. The matrix recording edge importance localizes brain regions and functional connections with significant aging and sex effects, which are verified by the neuroscience literature.

1 Introduction

The Blood-Oxygen-Level-Dependent (BOLD) signal of rs-fMRI characterizes the intrinsic functional organization of the human brain by measuring its spontaneous activity at rest [3]. One commonly used approach for identifying impact of factors, such as age and gender, on intrinsic functional networks is to predict their values by applying deep neural networks to the rs-fMRI of individual subjects [13,16,7,14]. Accurate predictors of those factors can then enhance the understanding of functional neurodevelopment across the life span [15], characterize developmental disruption caused by neurological disorders, and explain differences in cognitive performance linked to sex [22].

Selecting an appropriate network architecture for analyzing rs-fMRI data is not trivial. The (average) BOLD signal of each brain region is a structured time

* Equal contribution

series. A natural representation of such data are spatio-temporal graphs [24,25], where the temporal graph characterizes the dynamics of brain activity at each region, and the spatial graph characterizes the functional interaction between different brain regions. However, most existing deep learning works applied to rs-fMRI analysis fail to consider both aspects simultaneously. Methods that only incorporate spatial graph convolution [13,16,26] often transform the time series data into hand-crafted features, such as partial correlation, thereby potentially losing the fine temporal information of the BOLD signal. On the other hand, methods based on recurrent neural networks (RNN) [7,14,6] are designed to only learn temporal features from the data but neglect the spatial (functional) dependency between brain regions by viewing the BOLD signal at each time frame as an un-structured feature vector. To address these issues, we propose to use spatio-temporal Graph Convolution (ST-GC) [24,25] as a fundamental component for building deep neural networks for rs-fMRI analysis.

In computer vision, ST-GC Networks (ST-GCN) are popular for solving problems that base prediction on graph-structured time series [24,25,5]. In the context of rs-fMRI analysis, these networks have the potential to automatically extract features that jointly characterize functional connectivity patterns of the brain and their temporal dynamics within the BOLD series. To the best of our knowledge, we are the first to use ST-GCN for building predictive models based on rs-fMRI data. We train our network on short sub-sequences of BOLD time series to model the non-stationary nature of functional connectivity [19,28]. Further, we improve the interpretability of the model by learning an edge importance matrix associated with the ST-GC operation, which then can be used to identify selective functional connections significantly contributing to the prediction. We apply ST-GCN to predict the age and gender of healthy individuals of two large publicly available rs-fMRI datasets: Human Connectome Project (HCP, $N=1,096$) [20] and National Consortium on Alcohol and Neurodevelopment in Adolescence (NCANDA, $N=773$) [2]. The resulting prediction accuracy is significantly higher than traditional RNN-based methods. The optimal window size for the sub-sequences highly coincide between the two datasets despite their distinct imaging protocols and data processing pipelines. The learned edge importance can localize meaningful brain regions and functional connections with significant functional neurodevelopment and sexual differences.⁴

2 ST-GCN for rs-fMRI Analysis

We first relate functional networks to spatio-temporal graphs and then define the convolution ST-GC on it. Next, we introduce the architecture of our ST-GCN for rs-fMRI-based classification. Lastly, we describe the procedures for learning graph edge importance and training ST-GCN on short BOLD sequences.

Representing Functional Networks as Spatio-Temporal Graphs. We first assume the spontaneous activation of each region-of-interest (ROI) can be

⁴ The code is available at https://github.com/sgadgil6/cnslab_fmri

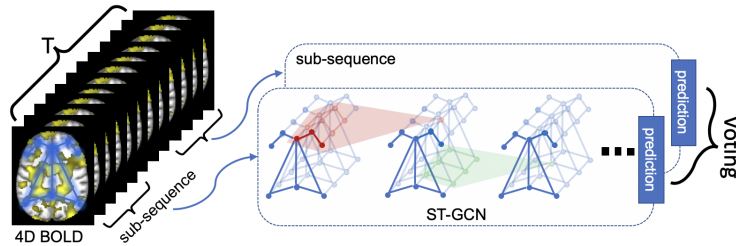


Fig. 1: Pipeline of our spatio-temporal graph convolutional network.

quantified by the average BOLD time series within that region. Such ROI-wise BOLD signal $\mathbf{f} \in \mathbb{R}^{N \times T}$ can then be defined on an undirected spatio-temporal graph $\mathcal{G} = (\mathcal{V}, \mathcal{E})$ (Fig. 1), where $\mathcal{V} = \{v_{t,i} | t = 1, \dots, T; i = 1, \dots, N\}$ are the set of nodes defined by N ROIs and T time points, and \mathcal{E} contains edges characterizing both temporal and spatial connections. Each edge in the temporal graph connects a ROI to the same ROI at the next time point. Each edge in the spatial graph (associated with a time point) connects two ROIs in accordance to the functional organization of the brain. While some existing works construct this spatial graph according to the topological arrangement among ROIs in the physical space (that only captures direct structural connections) [13], we instead define the affinity between any pair of ROIs as the magnitude of correlation between the two ROI-wise BOLD time series for the entire cohort (concatenating time series from all subjects). This practice can model interactions among ROIs that are distal in the physical space but similar in functional properties.

Spatio-temporal Graph Convolution (ST-GC). To define an ST-GC on such graphs, we denote $f_{in}(v_{ti})$ as the input feature at node v_{ti} and $B(v_{ti})$ as the spatio-temporal neighbourhood of v_{ti} , i.e.,

$$B(v_{ti}) = \{v_{qj} | d(v_{tj}, v_{ti}) \leq K, |q - t| \leq \lfloor \Gamma/2 \rfloor\}, \quad (1)$$

where K defines the *distance* of the spatial neighborhood (i.e., spatial kernel size) and Γ the temporal neighborhood (i.e., temporal kernel size). An ST-GC operation on node v_{ti} with respect to a convolutional kernel $\mathbf{w}(\cdot)$ and a normalization factor Z_{ti} can then be defined as [24]

$$f_{out}(v_{ti}) := \frac{1}{Z_{ti}} \sum_{v_{qj} \in B(v_{ti})} f_{in}(v_{qj}) \cdot \mathbf{w}(v_{qj}). \quad (2)$$

Adopting a similar implementation as in [24], we approximate the spatio-temporal convolutional kernel $\mathbf{w}(\cdot)$ by decomposing it to a spatial graph convolutional kernel $\mathbf{W}_{SG} \in \mathbb{R}^{C \times M}$ represented in the Fourier domain and a temporal convolutional kernel $\mathbf{W}_{TG} \in \mathbb{R}^{M \times \Gamma}$. Denote $\mathbf{f}_t \in \mathbb{R}^{N \times C}$ as the C -channel input features of the N ROIs at the t^{th} frame, $\mathbf{f}'_t \in \mathbb{R}^{N \times M}$ as the M -channel output features, and \mathbf{A} as the aforementioned affinity matrix. We first perform spatial graph convolution

at each time point by [11]

$$\mathbf{f}'_t = \mathbf{A}^{-\frac{1}{2}}(\mathbf{A} + \mathbf{I})\mathbf{A}^{-\frac{1}{2}}\mathbf{f}_t\mathbf{W}_{SG}, \quad (3)$$

where \mathbf{A} is a diagonal matrix of $A^{ii} = \sum_j A^{ij} + 1$. Then a temporal convolution is performed on the resulting features. Since the temporal graph has regular grid spacing, we perform a standard 1D convolution on the time series of features $\mathbf{f}_i \in \mathbb{R}^{M \times T}$ for each node v_i by $\mathbf{f}'_i = \mathbf{f}_i \otimes \mathbf{W}_{TG}$, where \otimes denotes convolution in the time domain, and $\mathbf{f}'_i \in \mathbb{R}^{M \times T'}$ is the final output of ST-GC for v_i .

Building an ST-GCN. We now introduce an architecture of ST-GCN for performing classification based on BOLD time series. As the first attempt to apply ST-GC to BOLD time series, we construct an ST-GCN composed of 3 layers of ST-GC units. The input to ST-GCN are 1-channel spatio-temporal features $\mathbf{f} \in \mathbb{R}^{N \times T}$ representing the BOLD signals extracted at N ROIs. Consistent with the setup in [24], each ST-GC layer produces 64-channel outputs with the temporal kernel size $\Gamma = 11$, a stride of 1, and a dropout rate of 0.5. Following the convolutional layers, a global average pooling produces a feature vector of length 64, which is then fed into a fully connected layer followed by sigmoid activation to get the class probabilities. The models are learned using stochastic gradient descent with a learning and weight decay rate of 0.001.

Learning Edge Importance. To determine the importance of spatial graph edges in the decision making, we integrate a positive and symmetric "edge importance" matrix $\mathbf{M} \in \mathbb{R}^{N \times N}$ into our model. This matrix is shared across all ST-GC layers and can be learned by replacing $\mathbf{A} + \mathbf{I}$ in Eq. (3) with $(\mathbf{A} + \mathbf{I}) * \mathbf{M}$ (element-wise multiplication). As such, while performing spatial graph convolution on node v_{ti} , the contribution from its neighbouring nodes $B(v_{ti})$ will be re-scaled according to the importance weights learned in the i^{th} row of \mathbf{M} . In this case, the diagonal entries of \mathbf{M} (self-connection) quantify importance for each ROI, and off-diagonal entries for each functional connection. Note that the original proposal by Yan et al. [24] learns an arbitrary and separate mask for each individual ST-GC layer. Their strategy generally results in negative, asymmetric masks that are difficult to interpret and vary across layers, while we enforce \mathbf{M} to be both positive and symmetric, making it more interpretable.

Training ST-GCN. We note that recent rs-fMRI studies have revealed that patterns of intrinsic functional connectivity are not stationary across the full rs-fMRI scan but exhibit considerable fluctuations. A widely applied approach for analyzing such dynamics is to divide the full rs-fMRI sequence into sub-sequences according to a fixed window size (often chosen empirically) and then to assess the connectivity within these segments. Accordingly, we also consider training ST-GCN on sub-sequences of window size T' sampled from the full data. Specifically, at each training iteration, we randomly sample a sub-sequence of length T' from the full sequence of each training subject in the mini-batch. At the testing stage, we sample S sub-sequences of length T' for each testing subject, derive the ST-GCN prediction for each sub-sequence, and perform a simple voting to produce the final subject-level prediction (e.g., the average of sigmoid values in the case of binary classification) (Fig. 1).

3 Experiments

NCANDA. Understanding the dramatic neurodevelopment and the emerging sexual differences during adolescence is an important topic in neuroscience [22,18]. Therefore, we first investigated the baseline NCANDA dataset, which publicly released the rs-fMRI scans (269 frames, TR=2s) of 773 subjects (ages 12-21, 388 young vs. 385 old adolescents, 376 male vs. 397 females). Among the 773 adolescents, 638 met the no-to-low alcohol drinking criteria of NIAAA (373 young vs. 265 old adolescents, 315 boys vs. 323 girls) [2]. Each rs-fMRI scan was preprocessed by the NCANDA pipeline, which registered the mean BOLD image to subject-specific T1 MRI and then non-rigidly registered to the standard MNI space [29]. The cortical surface was then parcellated to $N = 34$ ROIs according to [12]. The average BOLD signal in each ROI was normalized to z -scores.

HCP. The Human Connectome Project (HCP) S1200 [20] contains the rs-fMRI data for 1096 young adults (ages 22-35). We used the first session (15 min, $T = 1200$ frames, TR=0.72s) for each subject and excluded 5 rs-fMRIs with less than 1200 frames, resulting in the data of 498 females and 593 males. Each rs-fMRI went through the minimal processing pipeline of HCP, *fMRISurface* [9], which mapped each volume time series to the standard CIFTI grayordinates space. The cortical surface was parcellated to $N = 22$ major ROIs [8], and the average BOLD signal in each ROI was normalized to z -scores.

Experimental Setup. For the NCANDA dataset, we first tested ST-GCN for age classification (young vs. old) by performing 5-fold cross validation on the 773 rs-fMRIs. The training and testing were repeated on sub-sequences of different window sizes, from short segments of $T' = 16$ to the full sequence. The number of voters in the testing stage was fixed at $S = 64$. To ensure the prediction results were not confounded by alcohol drinking, the test accuracy was also recorded for the no-to-low drinking cohort, denoted as "ST-GCN-no-ex". Based on the optimal window size determined through cross validation, we trained the model on all subjects' data to produce an edge importance matrix summarizing the aging effects within the entire cohort. To reduce uncertainty in the estimation caused by stochastic gradient descent, we repeated the training 20 times and derived the "average" edge importance matrix as our final outcome. Next, the procedures of this aging analysis were repeated with respect to sex. For the HCP dataset, we only performed experiments with respect to sex, as the functional organization reaches maturity after young adulthood [23] and is unlikely to reveal any meaningful aging effect.

Baselines. We compared ST-GCN to baseline methods that are also based on end-to-end training on the BOLD time series. The first baseline was a Long Short-Term Memory (LSTM) model [10], a form of RNN frequently used to analyze rs-fMRI data [7,14]. Adopting a similar implementation as in [14], we designed an LSTM model with each recurrent cell having a hidden state of dimension 256. The output of the last hidden state was fed into a fully connected layer, with a dropout of 0.5, for the final classification. The second baseline, denoted as "GC-LSTM", only applied one layer of spatial graph convolution to extract features from the BOLD signal at each time frame. The features were then fed

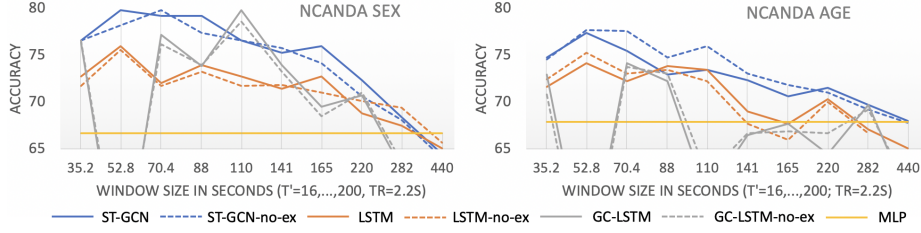


Fig. 2: Accuracy of age and sex prediction on the NCANDA dataset.

into an LSTM model for temporal analysis. This implementation improved over a Convolutional RNN [21], which used a 1D convolution to approximate the spatial graph convolution. The number of voters for these two LSTM-based methods were also fixed at $S=64$. Finally, to show the advantage of analyzing sub-sequences over the full-sequence analysis, we provided another simple baseline based on Multi-Layer Perceptron (MLP). The input to the network was a flattened vector of the upper triangular correlation matrix, which quantified the static functional connectivity between ROIs during the full scan. The MLP had 2 hidden layers, each with 64 neurons and ReLu activation.

4 Results and Analysis

NCANDA. Fig. 2 shows the prediction accuracy derived from the 5-fold cross validation for different methods. The accuracy scores measured on all NCANDA subjects were not significantly different from results on the no-to-low drinking cohort (denoted as “no-ex”, $p>0.5$), indicating that the predictions were not confounded by alcohol consumption in individuals. Compared to the MLP baseline that characterized static functional connectivity, all three deep-learning-based methods were generally more accurate when applied to shorter sub-sequences. ST-GCN achieved significantly higher accuracy than the two LSTM-based methods across different settings ($p<.0001$, two-sample t -test). For the LSTM baseline, varying the hidden-state dimension or adding more LSTM layers did not significantly improve its accuracy. For the GC-LSTM baseline, adding more convolution layers or increasing the number of feature channels reduced the accuracy substantially, which indicated that the strategy of training spatial graph convolution on each individual frame without incorporating temporal convolution was flawed. ST-GCN achieved the highest accuracy of 77.7% for age prediction at $T' = 24$ (52.8 s) and 79.8% for sex prediction at $T' = 32$ (70.4 s). The optimal range of T' for sex prediction was [24, 40] (52.8 - 88 s). These predictions were not confounded by subject motion based on the insignificant correlation between the prediction scores and the number of outlier frames in each rs-fMRI.

We visualized the edge importance matrices associated with the optimal models in Fig. 3. The images on the left (Fig. 3a+c) show the importance of each ROI

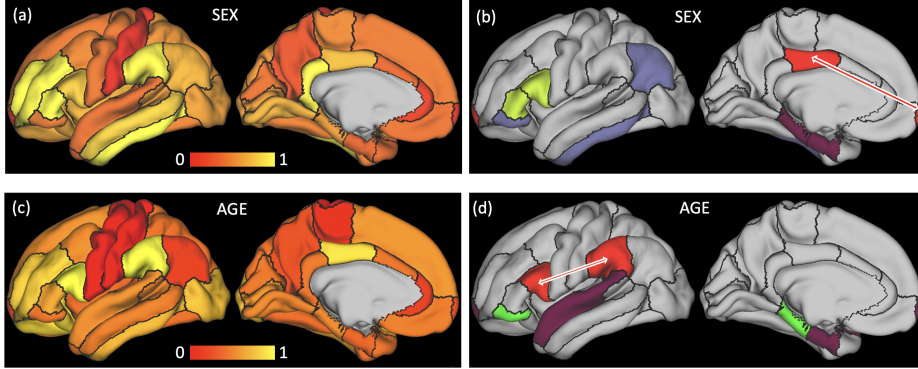


Fig. 3: Importance maps for age (a,b) and sex (c,d) prediction of the NCANDA study. (a,c): Importance of functional dynamics within each ROI; (b,d): Functional connections with importance higher than 0.3. Each connection is encoded by the same color between pairs of ROIs.

(diagonal entries) for prediction. Next, we visualized all functional connections (off-diagonal entries) with importance value higher than 0.3. For sex prediction, the most important ROI identified by ST-GCN was the inferior temporal lobe, which echoed findings from other resting-state studies [4] and from a structural MRI analysis on the NCANDA cohort [27]. We also identified a significant effect in the frontal-posterior-cingulate (PCC) connection (red in Fig. 3b), which defines the default mode network, a signature intrinsic network frequently linked to sexual differences [17]. For age prediction, the most critical ROIs were the supramarginal and par opercularis regions (Fig. 3c). Their functional interaction (Fig. 3d), which defined a major part of the inferior temporo-parieto-frontal network, was shown to decrease in older adolescents within the NCANDA cohort by a longitudinal rs-fMRI study [29]. All the results above demonstrate that our strategy of edge importance learning can accurately localize functional properties of the brain related to significant aging and sex effects.

HCP. Fig. 4a shows the accuracy for sex prediction on the HCP dataset. To put our analysis into context, we also listed results from prior studies by Weis et al. [22] and Smith et al. [18] on sex classification of HCP subjects. These works applied linear classifiers and used correlation coefficients as input features respectively, which was similar to our MLP baseline. Note that their results can not be strictly compared to ours as different cohorts and data processing pipelines were used for analysis⁵. However, the sub-optimal accuracy of our MLP baseline together with the prior results supports that the dynamical properties of functional interactions among brain regions can not be fully captured by the static correlation coefficients and requires more comprehensive spatio-temporal modeling.

⁵ the 87% accuracy in [18] on 131 HCP subjects was based on multi-modal data

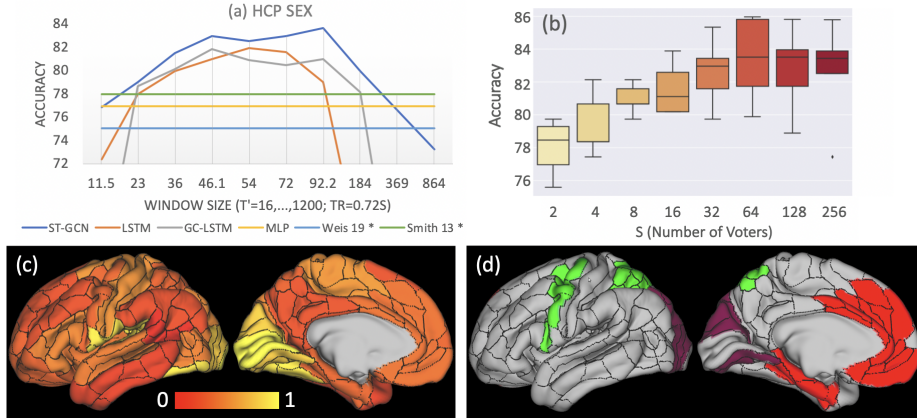


Fig. 4: Experiments on HCP: (a) Sex prediction accuracy w.r.t window size. * denotes results from prior studies. (b) Distribution of prediction accuracy scores from cross validation w.r.t. the number of voters. (c,d) Importance maps for sex prediction.

Deep-learning-based methods, on the other hand, achieved more accurate predictions on sub-sequences of $T' \in [32, 128]$ (23.04 - 92.16 s), and ST-GCN produced higher accuracy than the two LSTM-based methods across all window sizes. ST-GCN achieved the highest accuracy of 83.7% at $T' = 128$ (92.16 s). Increasing the number of voters did not further increase testing accuracy (Fig. 4b). Moreover, ST-GCN produced similarly optimal accuracy scores for $T' \in [64, 128]$ (46.08 - 92.16 s). This range was highly consistent with the one revealed in the NCANDA experiment despite the difference in imaging protocols, length of BOLD signal, brain parcellation, and data processing pipelines between the two studies. These results converge with recent understanding in neuroscience literatures that states of dynamical functional connectivity should be quantified within short time windows. [1,19]. By visualizing the edge importance matrix derived from the HCP subjects, we found that regions with significant sexual differences in young adults were spatially more concentrated compared to adolescents (the NCANDA experiment) and mainly located in the visual cortex (Fig. 4c). This phenomenon could be potentially linked to the evidence that sexual dimorphism in intrinsic functional organization diminishes with age (sex-age interaction) during adolescence [17].

5 Conclusion

We introduced a framework for analyzing rs-fMRI data based on spatio-temporal graph convolution networks. By analyzing the rs-fMRI data of two large-scale neuroimaging studies, we showed that ST-GCN could accurately predict age and gender of the study participants based on short sequences of BOLD time

series. The similar optimal window sizes (of the sub-sequences) between the two datasets showcased the effectiveness of ST-GCN in analyzing dynamic functional connectivity. Further, our strategy for learning graph edge importance within the context of model interpretation could be potentially valuable for advancing knowledge in neuroscience.

References

1. Allen, E., Damaraju, E., Plis, S., Erhardt, E., Eichele, T., Calhoun, V.: Tracking whole-brain connectivity dynamics in the resting state. *Cerebral Cortex* **24**(3), 663–676 (2014). <https://doi.org/10.1093/cercor/bhs352>
2. Brown, S., Brumback, T., Tomlinson, K., et al.: The national consortium on alcohol and neurodevelopment in adolescence (NCANDA): A multisite study of adolescent development and substance use. *J Stud Alcohol Drugs*. **76**(6), 895–908 (2015). <https://doi.org/10.15288/jsad.2015.76.895>
3. Buckner, R., Krienen, F., Yeo, B.: Opportunities and limitations of intrinsic functional connectivity MRI. *Nat Neurosci*. **16**(7), 832–837 (2013). <https://doi.org/10.1038/nn.3423>
4. Conrin, S.D., Zhan, L., Morrissey, Z.D., Xing, M., Forbes, A., Maki, P., Milad, M.R., Ajilore, O., Langenecker, S.A., Leow, A.D.: From default mode network to the basal configuration: Sex differences in the resting-state brain connectivity as a function of age and their clinical correlates. *Frontiers in Psychiatry* **9**, 365 (2018). <https://doi.org/10.3389/fpsy.2018.00365>
5. Covert, I., Krishnan, B., Najm, I., Zhan, J., Shore, M., Hixson, J., Po, M.J.: Temporal graph convolutional networks for automatic seizure detection. In: *Machine Learning for HealthCare* (2019)
6. Cui, Y., Zhao, S., Wang, H., Xie, L., Chen, Y., Han, J., Li, K., Zhou, F., Liu, T.: Identifying Brain Networks of Multiple Time Scales via Deep Recurrent Neural Network: 21st International Conference, Granada, Spain, September 16-20, 2018, Proceedings, Part III, pp. 284–292 (09 2018). https://doi.org/10.1007/978-3-030-00931-1_33
7. Dvornek, N., Ventola, P., Pelphrey, K., Duncan, J.: Identifying autism from resting-state fmri using long short-term memory networks. vol. 10541, pp. 362–370 (09 2017). https://doi.org/10.1007/978-3-319-67389-9_42
8. Glasser, M., Coalson, T., Robinson, E., Hacker, C., Harwell, J., Yacoub, E., Ugurbil, K., Andersson, J., Beckmann, C., Jenkinson, M., Smith, S., Van Essen, D.: A multi-modal parcellation of human cerebral cortex. *Nature* **536** (07 2016). <https://doi.org/10.1038/nature18933>
9. Glasser, M., Sotiropoulos, S., Wilson, J., Coalson, T., Fischl, B., Andersson, J., Xu, J., Jbabdi, S., Webster, M., Polimeni, J., DC, V., Jenkinson, M.: The minimal preprocessing pipelines for the human connectome project. *NeuroImage* **80**, 105 (10 2013). <https://doi.org/10.1016/j.neuroimage.2013.04.127>
10. Hochreiter, S., Schmidhuber, J.: Long short-term memory. *Neural computation* **9**(8), 1735–1780 (1997)
11. Kipf, T.N., Welling, M.: Semi-supervised classification with graph convolutional networks. In: *ICLR* (2017)
12. Klein, A., Tourville, J.: 101 labeled brain images and a consistent human cortical labeling protocol. *Frontiers in Neuroscience* **6**, 171 (2012). <https://doi.org/10.3389/fnins.2012.00171>

13. Ktena, S.I., Parisot, S., Ferrante, E., Rajchl, M., Lee, M., Glocker, B., Rueckert, D.: Distance metric learning using graph convolutional networks: Application to functional brain networks. In: MICCAI (09 2017). https://doi.org/10.1007/978-3-319-66182-7_54
14. Li, H., Fan, Y.: Brain Decoding from Functional MRI Using Long Short-Term Memory Recurrent Neural Networks: 21st International Conference, Granada, Spain, September 16-20, 2018, Proceedings, Part III, vol. 11072, pp. 320–328 (09 2018). https://doi.org/10.1007/978-3-030-00931-1_37
15. Li, H., Satterthwaite, T.D., Fan, Y.: Brain age prediction based on resting-state functional connectivity patterns using convolutional neural networks. In: ISBI (2018)
16. Li, X., Dvornek, N.C., Zhou, Y., Zhuang, J., Ventola, P., Duncan, J.S.: Graph neural network for interpreting task-fmri biomarkers. In: Medical Image Computing and Computer-Assisted Intervention (2019)
17. Müller-Oehring, E., Kwon, D., Nagel, B., Sullivan, E., Chu, W., Rohlfing, T., Prouty, D., Nichols, B., Poline, J.B., Tapert, S., Brown, S., Cummins, K., Brumback, T., Colrain, I., Baker, F., de Bellis, M., Voyvodic, J., Clark, D., Pfefferbaum, A., Pohl, K.: Influences of age, sex, and moderate alcohol drinking on the intrinsic functional architecture of adolescent brains. *Cerebral cortex (New York, N.Y. : 1991)* **28**, 1–15 (02 2017). <https://doi.org/10.1093/cercor/bhx014>
18. Smith, S.M., Vidaurre, D., Beckmann, C.F., et al.: Functional connectomics from resting-state fmri. *Trends Cogn Sci* **17**(12), 666–682 (2013)
19. Taghia, J., Ryali, S., et al.: Bayesian switching factor analysis for estimating time-varying functional connectivity in fmri. *NeuroImage* **155**, 271–290 (2017). <https://doi.org/10.1016/j.neuroimage.2017.02.083>
20. Van Essen, D.C., Smith, S.M., Barch, D.M., Behrens, T.E., Yacoub, E., Ugurbil, K., Consortium, W.M.H., et al.: The wu-minn human connectome project: an overview. *Neuroimage* **80**, 62–79 (2013)
21. Wang, L., Li, K., Chen, X., Hu, X.: Application of convolutional recurrent neural network for individual recognition based on resting state fmri data. *Frontiers in Neuroscience* **13** (05 2019). <https://doi.org/10.3389/fnins.2019.00434>
22. Weis, S., Patil, K.R., Hoffstaedter, F., Nostro, A., Yeo, B.T.T., Eickhoff, S.B.: Sex classification by resting state brain connectivity. *Cerebral Cortex* (2019). <https://doi.org/10.1093/cercor/bhz129>
23. Westlye, L., Walhovd, K., Dale, A., Bjørnerud, A., Due-Tønnessen, P., Engvig, A., Grydeland, H., Tamnes, C., Ostby, Y., Fjell, A.: Life-span changes of the human brain white matter: Diffusion tensor imaging (dti) and volumetry. *Cerebral cortex (New York, N.Y. : 1991)* **20**, 2055–68 (09 2010). <https://doi.org/10.1093/cercor/bhp280>
24. Yan, S., Xiong, Y., Lin, D.: Spatial temporal graph convolutional networks for skeleton-based action recognition. In: AAAI (2018)
25. Yu, B., Yin, H., Zhu, Z.: Spatio-temporal graph convolutional networks: A deep learning framework for traffic forecasting. In: IJCAI (2018)
26. Zhang, Y., Bellec, P.: Functional annotation of human cognitive states using graph convolution networks. In: NeurIPS 2019 Workshop Neuro AI (2019)
27. Zhao, Q., Adeli, E., Pfefferbaum, A., Sullivan, E., Pohl, K.: Confounder-aware visualization of convnets (10 2019). https://doi.org/10.1007/978-3-030-32692-0_38
28. Zhao, Q., Honnorat, N., Adeli, E., Pfefferbaum, A., Sullivan, E.V., Pohl, K.M.: Variational autoencoder with truncated mixture of gaussians for functional connectivity analysis. In: Information Processing in Medical Imaging. LNCS, vol. 11492, pp. 867–879. Springer (2019). https://doi.org/10.1007/978-3-030-20351-1_68

29. Zhao, Q., Kwon, D., Müller-Oehring, E., Le Berre, A.P., Pfefferbaum, A., Sullivan, E., Pohl, K.: Longitudinally consistent estimates of intrinsic functional networks. *Human Brain Mapping* **40** (02 2019). <https://doi.org/10.1002/hbm.24541>